Translational Oncology
www.transonc.com

Volume 12 Number 9 September 2019 pp. 1229–1236 1229

Building CT Radiomics-Based Models for Preoperatively Predicting Malignant Potential and Mitotic Count of Gastrointestinal Stromal Tumors

Chao Wang[*,1], Hailin Li[†,‡,1], Yeerfan Jiaerken[*], Peiyu Huang[*], Lifeng Sun[§], Fei Dong[*], Yajing Huang[¶], Di Dong[†,‡], Jie Tian[†,#,] and Minming Zhang[*]**

[*]Department of Radiology, the Second Affiliated Hospital, Zhejiang University School of Medicine, Hangzhou, China;
[†]CAS Key Lab of Molecular Imaging, Institute of Automation, Chinese Academy of Sciences, Beijing, China
[‡]University of Chinese Academy of Sciences, School of Artificial Intelligence, Beijing, China
[§]Department of Surgical Oncology, the Second Affiliated Hospital, Zhejiang University School of Medicine, Hangzhou, China
[¶]Department of Pathology, the Second Affiliated Hospital, Zhejiang University School of Medicine, Hangzhou, China;
[#]Beijing Advanced Innovation Center for Big Data-Based Precision Medicine, School of Medicine, Beihang University, Beijing, China
[**]Engineering Research Center of Molecular and Neuro Imaging of Ministry of Education, School of Life Science and Technology, Xidian University, Xi'an, China

Abstract

PURPOSE: To build radiomic prediction models using contrast-enhanced computed tomography (CE-CT) to preoperatively predict malignant potential and mitotic count of gastrointestinal stromal tumors (GISTs). *PATIENTS AND METHODS*: A total of 333 GISTs patients were retrospectively included in our study. Radiomic features were extracted from the preoperative CE-CT images. According to postoperative pathology, patients were categorized by malignant potential and mitotic count, respectively. The most valuable radiomic features were chosen to build a logistic regression model to predict the malignant potential and a random forest classifier model to predict the mitotic count. The performance of radiomic models was assessed with the receiver operating characteristics curve. Our study further developed a radiomic nomogram to preoperatively predict malignant potential in a personalized way for patients with GISTs. *RESULTS*: The predictive model was built to discriminate high– from low–malignant potential GISTs with an area under the curve (AUC) of 0.882 (95% CI 0.823-0.942) in the training set and 0.920 (95% CI 0.870-0.971) in the validation set. Moreover, the other radiomic model was built to differentiate high– from low–mitotic count GISTs with an AUC of 0.820 (95% CI 0.753-0.887) in the training set and 0.769 (95% CI 0.654-0.883) in the validation set. *CONCLUSION*: The radiomic models using CE-CT showed a good predictive performance for preoperative risk stratification of GISTs and hold great potential for personalized clinical decision making.

Translational Oncology (2019) 12, 1229–1236

Address all correspondence to: Minming Zhang, PhD, MD, Department of Radiology, the Second Affiliated Hospital, Zhejiang University School of Medicine, NO.88 Jiefang Road, Hangzhou 310009, China; or Jie Tian, PhD, Director of the CAS Key Laboratory of Molecular Imaging, Institute of Automation, Chinese Academy of Sciences, Beijing, 100190 China; or Di Dong, PhD, CAS Key Laboratory of Molecular Imaging, Institute of Automation, Chinese Academy of Sciences, Beijing, 100190 China. E-mails: zhangminming@zju.edu.cn (M. Zhang); jie.tian@ia.ac.cn (J. Tian) di.dong@ia.ac.cn (D. Dong)

[1] Chao Wang and Hailin Li contributed equally to this work

Received 3 April 2019; Revised 13 June 2019; Accepted 17 June 2019

1936-5233/19
https://doi.org/10.1016/j.tranon.2019.06.005

Introduction

Gastrointestinal stromal tumors (GISTs) are the most common subgroup of gastrointestinal mesenchymal neoplasms with fusoid and epitheliod cells or rarely with pleomorphic cells [1], and arise from Cajal interstitial cells or their similar cells [2,3]. The diagnosis of GISTs is histopathological and implemented by the immunohistochemical marker CD117 (or C-KIT) and DOG1 [3–5]. Nearly 50%-70% of GISTs originate from the stomach and 30%-45% from the small bowel [6,7]. The biological behavior of GISTs varies from benign to malignant, which is different from other solid lesions of the gastrointestinal tract. Malignant GISTs tend to recur and metastasize even after a complete surgical resection [8]. The National Institutes of Health (NIH) risk categories criteria of proposed modification (Table S1) and the National Comprehensive Cancer Network (NCCN) prognosis prediction guidelines (Table S2) are widely used in clinical practice due to their important value for assessment of prognosis after operation. GISTs are classified into four risk categories, ranging from very low risk to high risk, which are determined by the tumor size, tumor location (gastric or nongastric), and mitotic count [3,9]. The recurrent rates vary from 2.4% to 69.8% in different risk categories of GISTs [10]. In the NIH criteria (Table S1) and NCCN guidelines (Table S2), the morphological features of tumor size and mitotic count gain the greatest acceptance as predictors of malignant outcome. Nevertheless, these pathological evaluations of surgical specimens are only available postoperatively. It is relatively easy to calculate the tumor size preoperatively using anatomic imaging techniques, but it is difficult to calculate the mitotic count preoperatively. Thus, the determination of malignant potential of GISTs remains difficult. However, it is of high clinical value to predict malignant potential of GISTs preoperatively, which may offer guidelines for determining the need for adjuvant chemotherapy, such as the use of molecular targeted drugs for preventing metastasis and recurrence [11]. Previous studies further confirmed that the prognosis of advanced primary GISTs patients could be improved by preoperative targeted drugs treatment [12–14]. Therefore, preoperative prediction of malignant potential can provide valuable clues for predicting disease prognosis and determining the need for adjuvant therapy.

Radiomics can be used to quantify tumor phenotypic characteristics in detail and comprehensively because of its high-throughput extraction of radiomic features quantifying tumor's shape, intensity, and texture from medical images [15,16]. The radiomic approach has been widely used for lesion detection, preoperative diagnosis of disease status, preoperative prognostic evaluation, prediction of treatment response, and prediction of disease-free survival [17–21]. Contrast-enhanced computed tomography (CE-CT) is a fundamental imaging tool for detecting the lesion and staging and for the assessment of treatment response in clinical practice of GISTs [3,22,23]. In this study, two radiomic models based on preoperative CE-CT were built and validated to predict the malignant potential and mitotic count of GISTs, respectively.

Materials and Methods

Patients

The present study was approved by the Institutional Review Boards of the Second Affiliated Hospital of Zhejiang University School of Medicine. We searched our retrospectively maintained database for consecutive patients who underwent preoperative CE-CT between June 2009 and March 2018. The inclusion criteria included 1) histological diagnosis of GISTs; 2) availability of preoperative CE-CT; and 3) histological analysis of the surgical specimen reporting the lesion size, location of origin, and the mitotic index. The exclusion criteria included 1) patients who received preoperative chemotherapy, such as the use of targeted drugs, and 2) tumor ruptured during the surgery. The final number of patients who matched the above criteria and were enrolled in the study was 333 (172 men and 161 women; mean age, 58.8 ± 11.8 years).

Pathology

Postoperative specimens were fixed with formalin and then stained with hematoxylin and eosin. Immunohistochemical staining of tumors for c-kit and CD34 or both was diagnosed as GISTs. Mitotic count was calculated on 50 high-power fields (HPFs). Neoplasm size was measured on formalin-fixed sample. According to the NIH criteria (Table S1), GISTs were classified into four risk grades, ranging from very low risk to high risk. According to risk categories, the patients in this study were categorized as the low– (very low to intermediate risk) and the high–malignant potential group (high risk). In addition, according to mitotic count, the patients with mitotic count ≤5/50 HPF were categorized as the low–mitotic count group, and the patients with mitotic count >5/50 HPF were categorized as the high–mitotic count group.

CT Protocol

All patients underwent abdominal CE-CT. Details of the acquisition parameters and CT image retrieval procedures were provided in Supplementary S1.

Radiomic Feature Extraction

CE-CT images in the portal venous phase were used for tumor segmentation since the portal venous phase had a better performance in identifying the lesion from the surrounding normal tissue. The tumor outline at the largest cross-sectional area was drawn as the region of interest (ROI) by an experienced radiologist who had no knowledge of the tumors other than their locations by using a free open-source software package (ITK-SNAP, version 3.6.0; http://itksnap.org) to provide the ROI for computer-based image analysis (Figure 1).

Radiomic feature extraction procedures were provided in Supplementary S2. A total of 385 quantitative parameters from feature sets of Histogram, Form Factor, Haralick [24], Gray-Level Co-occurrence Matrix [24], and Run-Length Matrix [25,26] were used in our image feature extraction.

To evaluate inter- and intraobserver reproducibility, 30 cases were chosen at random for ROI delineation and ROI-based feature extraction by two experienced radiologists (radiologist 1 and radiologist 2). To find out robust radiomic features, we used inter- and intraclass correlation coefficient (ICC) to evaluate the stability and reproducibility in radiomic feature extraction. The intraobserver ICC was calculated based on the twice feature extractions by radiologist 1. The interobserver ICC was calculated based on the first-extracted features by radiologist 1 and those by radiologist 2. In general, ICC > 0.75 was deemed to have a good reliability or reproducibility [27].

Statistical Analysis

Clinicopathologic Characteristics

The groups' differences in gender, age, tumor location, malignant potential, and mitotic count were compared using two-sample t or χ^2 test in SPSS 20.0 software (IBM).

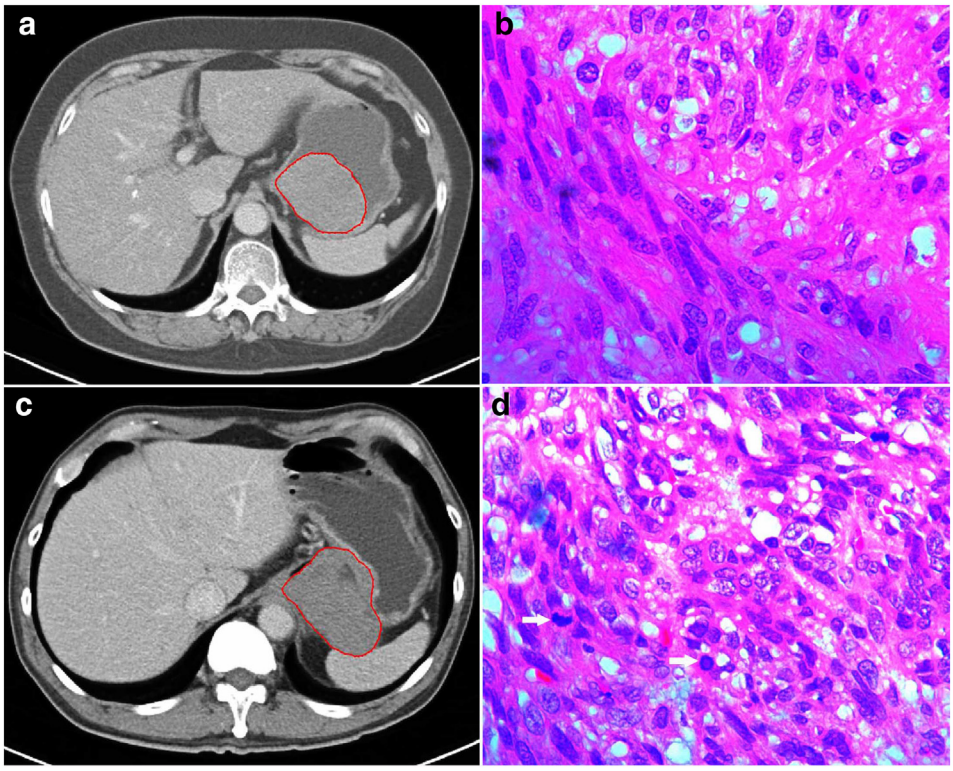

Figure 1. (A, C) The tumor outline at the largest cross-sectional area was manually drawn as the ROI (red circle). (A, B) A gastric lesion with a low mitotic rate (≤5/HPFs). A 67-year-old female patient with a gastric lesion, 6.2 cm in size, 0 mitosis/50 HPFs, belonging to the moderate-risk class. (C, D) A gastric lesion with a high mitotic rate (>5/HPFs). A 61-year-old male patient with a gastric exophytic lesion, 6.9 cm in size, 31 mitoses/50 HPFs (arrows), belonging to the high-risk class.

Radiomic Feature Selection and Radiomic Model Building

As tumor location is a main component of the modified NIH criteria [9] (Table S1), we further combined tumor location and the radiomic features into a feature set. Data preprocessing was performed on this feature set in the following three steps. First, abnormal values were replaced with median. Second, data were partitioned at random: the training set accounted for 0.7, and the validation set accounted for 0.3. Third, standardization was done before analysis (Supplementary S3).

Feature selection was performed in the following three steps to reduce redundancy. Firstly, the difference of every radiomic feature between the high– and low–malignant potential groups was compared using χ^2 test and Mann-Whitney U test (MW). Secondly, a minimum redundancy maximum relevance (mRMR) feature ranking was calculated, and one-third of features were retained, which reduced the redundancy between features in the feature subset. The mRMR feature ranking takes into account not only the correlation between features and labels but also the redundancy between features [28]. Thirdly, the least absolute shrinkage and selection operator method (LASSO) was performed to select the most valuable predictive features, and backward stepwise was used to select high-risk related optimum feature subset. As a widely used machine learning method in the field of radiomics, the LASSO method selects a suitable number of non–zero-weighted features according to the minimum or 1-standard error 1-SE criteria, which can prevent overfitting in the model construction. Finally, the remaining features were selected to build a radiomic model to predict the malignant potential using a logistic regression classifier. In addition, in the process of selecting related optimum features subset for the high–/low–mitotic count groups, the feature selection was also performed in three steps to reduce redundancy (Supplementary S4).

Predictive Performance of Radiomic Model

The radiomic model performance was evaluated by receiver operating characteristic (ROC) curves. To quantify the discriminatory power of the radiomic model, the parameters including the area under the curve (AUC), sensitivity, specificity, and accuracy were provided. Then, the same parameters on the validation set were obtained from the training set to test the prediction performance of this model. R software (version 3.5.0; http://www.R-project.org) was

Table 1. Characteristics of Patients in the Training and Validation Sets

Characteristic	Training Set	Validation Set	*P*
Gender			.693
Male	122	50	
Female	111	50	
Age (mean ± SD) (y)	57.8 ± 12.1	60.9 ± 11.0	.03
Tumor location			.124
Stomach	149	55	
Small intestine	84	45	
Malignant potential			.096
Low malignant potential	166	62	
High malignant potential	84	38	
Mitotic count			.995
≤5/50 HPF	184	79	
>5/50 HPF	49	21	

Independent-samples t test was applied in continuous variables. χ^2 test was applied in categorical variables. The number in the table is the number of the patients except the age.
P value <.05.

applied in the above statistical analysis. All of the statistical tests in this study were two-tailed, and the R packages used in this study were shown in Supplementary S5.

Results

Patient Characteristics

Three hundred and thirty-three patients were comprised of men (172 cases) and women (161cases), stomach (204 cases) and small intestine (129 cases), the low malignant potential (228 cases) and the high malignant potential (105 cases), and the low mitotic count (263 cases) and the high mitotic count (70 cases). The training set consisted of 122 men and 111 women (57.8 ± 12.1 years, range 16-88 years). The validation set consisted of 50 men and 50 women (60.9 ± 11.0 years, range 21-86 years). A statistical difference in age between the two sets (P = .03) was found, but no statistical differences were found in gender (P = .693), tumor location (P = .124), malignant potential (P = .096), and mitotic count (P = .995) between the two sets. The clinicopathologic characteristics of gender, age, tumor location, malignant potential, and mitotic count of the two sets were summarized in Table 1. Demographic characteristics of high–/low–malignant potential groups and high–/low–mitotic count groups in the two sets were summarized in Supplementary S6 and Tables S3 and S4.

Reproducibility of Radiomic Feature Extraction

A total of 385 radiomic features were extracted from patients with GISTs. The feature with ICC > 0.75 was deemed to have a good reliability or reproducibility in both inter- and intraobserver analyses. As a result, a total of 378 features were robust and then applied for subsequent feature selection.

Feature Selection and Radiomic Model Building

The High– and Low–Malignant Potential Groups. First, χ^2 test and MW were performed to compare the feature differences between the high–/low–malignant potential groups, and 265 features remained. Second, an mRMR feature ranking was calculated, and 90 features remained. Last, a LASSO method (Figure 2) with cross-validation was performed, and five features remained. Finally, the three features including tumor location, maximum diameter, and a texture feature were selected after backward stepwise, and then the remaining three features were chosen to build a radiomic model by a logistic regression model. The three selected features were provided in Table 2.

The High– and Low–Mitotic Count Groups. First, one-way analysis of variance and MW were used to compare the difference in each radiomic feature between the low– and the high–mitotic count groups, and 239 features remained. Second, a correlation analysis (Spearman's correlation test) between each two different features was performed, and 61 features remained. Lastly, a LASSO method with cross-validation was performed, and 14 features remained. Finally, the remaining 14 features were chosen to build a radiomic model using a random forest classifier. The 14 selected features were provided in Table 3.

Predictive Performance of Radiomic Model

The High– and Low–Malignant Potential Groups. In the training set, the radiomic model had an excellent discrimination capacity (AUC =0.882, 95% confidence interval [CI]: 0.823-0.942; sensitivity = 80.6%; specificity = 94%; and accuracy = 90.1%) for discriminating the high– from the low–malignant potential GISTs (Figure 3*A*). In the validation set, this radiomic model had a similar discrimination capacity (AUC = 0.920, 95% CI: 0.870-0.971; sensitivity = 76.3%; specificity = 88.7%; and accuracy = 84%) (Figure 3*B*). Finally, the selected three features, including maximum diameter, intensity values range, and tumor location (Table 2), were incorporated into the radiomic nomogram building (Figure 4).

The High– and Low Mitotic Count Groups. In the training set, the radiomic model had a satisfactory discrimination capacity (AUC = 0.820, 95% CI: 0.753-0.887; sensitivity =63.3%; specificity =91.3%;

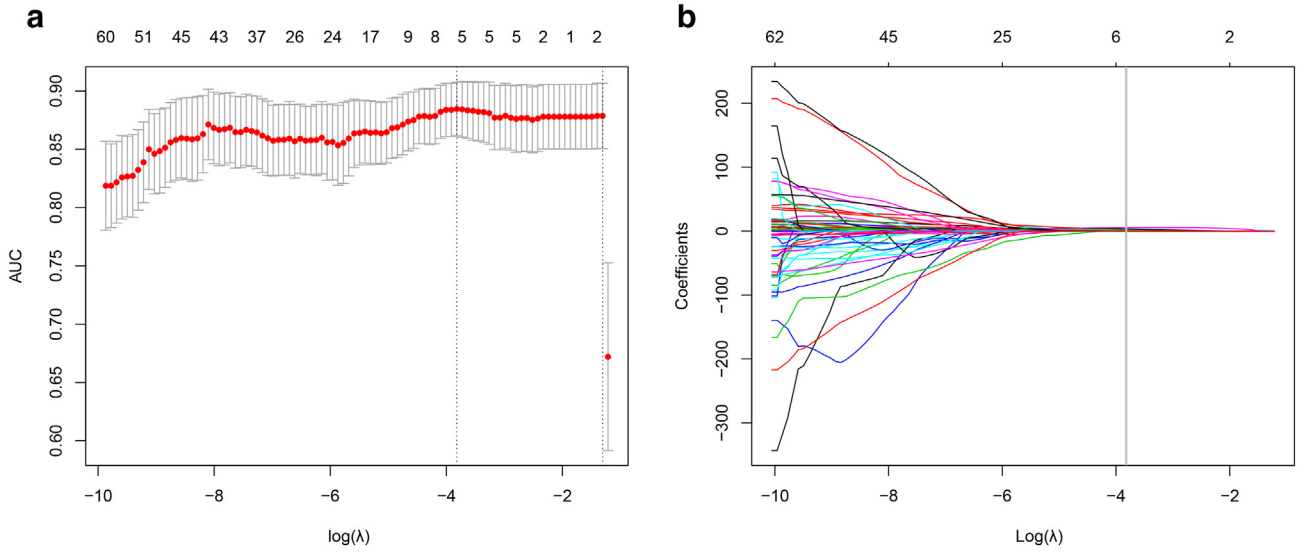

Figure 2. Feature selection in the malignant potential groups with the LASSO method. This method minimized the sum of squares of residues, with the sum of the absolute values of the selected features coefficients being not more than a tuning parameter (λ). (A) Tuning parameter (λ) selection using LASSO penalized logistic regression with 10-fold cross-validation. The AUC was plotted versus log (λ). (B) LASSO coefficient profiles of the radiomic features. A coefficient profile plot was plotted versus the log (λ). Each colored line represents the coefficient of each feature. Vertical line was drawn at the selected λ, where five features had nonzero coefficients.

Table 2. Selected Features with Descriptions of the High– and Low–Malignant Potential Groups

Feature Name	Description
Tumor location	Gastric or nongastric
Maximum diameter	Measures the size of the tumor region
Intensity values range	Represents the range of intensity values

and accuracy = 85.4%) for discriminating the high– from the low–mitotic count groups (Figure 5*A*). In the validation set, this radiomic model had a similar discrimination capacity (AUC = 0.769, 95% CI: 0.654-0.883; sensitivity = 52.4%; specificity = 81%; and accuracy = 75%) (Figure 5*B*).

Discussion

In this study, we developed and validated an effectively preoperative radiomic model using CE-CT to differentiate the high– from the low–malignant potential GISTs, and we further built a personalized radiomic nomogram to predict malignant potential for patients with GISTs. Moreover, we also developed and validated a radiomic model to differentiate the high– from the low–mitotic count GISTs. The present research confirmed the predictive ability of radiomic model for both malignant potential and mitotic count of GISTs, and it may be a potential imaging method for assessing prognosis and guiding clinical treatment decision making before surgery in a noninvasive way.

Despite complete surgical resection, up to 50% of GISTs will recur at a median of 24 months [29]. Accurate preoperative risk grade classification for patients with GISTs has gained a lot of attention due to the emergence of targeted drugs [11,30]. A previous CE-CT study [31] investigated the associations between imaging features, mitotic count, and risk categories and found that some imaging features, including heterogeneous enhancement, angiogenesis, necrosis, adjacent organ invasion, and irregular margins, were correlated with the high-risk category. Meanwhile, irregular margins and adjacent organ invasion were associated with the high mitotic count. It should be noted that these imaging findings were judged by radiologists' subjective analysis, and this qualitative analysis would bring about inter- and intraobserver variability. However, in our present study, quantitative radiomic features were extracted and selected to build a radiomic model which could effectively avoid inter- and intraobserver variability.

Table 3. Selected Features with Descriptions of the Low– and High–Mitotic Count Groups

Feature Name	Description
Intensity values range	Represents the range of intensity values
Sphericity	Measures the shape in the ROI
Voxel value sum	Represents the sum calculations for voxels in the ROI
Uniformity	Represents a histogram parameter
Inverse difference moment_AllDirection_offset1_SD	Inverse difference moment is the local homogeneity.
Inverse difference moment_angle0_offset4	
Inverse difference moment_angle45_offset4	
Inverse difference moment_angle90_offset4	
Inverse difference moment_angle135_offset4	
Inverse difference moment_angle0_offset7	
Inverse difference moment_angle90_offset7	
Correlation_angle135_offset7	Correlation measures the similarity of the gray levels in neighboring pixels
Long run high gray level emphasis_All Direction_offset1_SD	Represents a feature of gray level run-length matrix
Short run emphasis_All Direction_offset4_SD	Represents a feature of gray level run-length matrix

Note: Suffix of "0," "45," "90," and "135" means the directions of gray-level matrix directions.

Positron-emission tomography/computed tomography (PET/CT) can assess tumor anatomy and glucose metabolism and has been considered as an important imaging tool for GISTs [32–34]. Tokumoto et al. [34] used PET/CT to discriminate the high from low malignant potential of GISTs, and they found that PET/CT might be useful for evaluating the risk category of GISTs (sensitivity = 85.7%, specificity = 62.5%) but could not be used for evaluating the mitotic count. Our present study built a CT-based radiomic model with a similar prediction performance with a sensitivity of 76.3% and a specificity of 88.7%. Furthermore, in our study, we further developed and validated a CT-based radiomic model to differentiate the high– from the low–mitotic count GISTs with a diagnostic accuracy of 75%. In addition, Wong et al. [35] compared the performance between magnetic resonance imaging (MRI) and PET/CT of GISTs, and they reported that diffusion weighted imaging had a similar performance as PET/CT in diagnosis and treatment response evaluation for patients with GISTs. In fact, CE-CT is the most routinely used imaging examination tool for GISTs patients, while PET/CT or MRI is regarded as an additional imaging examination tool because PET/CT and MRI examinations are relatively expensive and take a long time [3]. Therefore, CT-based radiomic model in discriminating malignant potential of GISTs could have better generalizability and clinical application value.

In the present study, we used the three selected features, including tumor location and maximum diameter and intensity values range, to develop a radiomic model and an individualized radiomic nomogram for discriminating malignant potential of GISTs. Malignant potential of GISTs is commonly stratified based on tumor size, tumor location (gastric or nongastric), and mitotic count [3,9,36–39]. Tumor size is an important factor for assessing the malignant potential and prognosis of GISTs (Tables S1 and S2). The NCCN guideline has recommended that the tumor should be surgically resected when tumor size is larger than 2 cm, and the tumor can be resected or monitored by endoscopy when tumor size is smaller than 2 cm [40]. However, it is insufficient to discriminate the high– from the low–malignant potential GISTs simply only by tumor size since some GISTs with small size may be high-risk malignancy and have poor prognosis [41,42]. Tumor location is another important factor for prognosis evaluation and is a main component of the modified NIH criteria [9] (Table S1). The small intestine GISTs have been reported to be more aggressive and have worse prognosis than gastric GISTs of the same size [43,44]. In this study, tumor size and tumor location were significantly different between the high– and low–malignant potential groups, and as expected, these two factors finally remained after a series of radiomic feature selections in the radiomic model. Tumor size can be measured and tumor location can be determined by conventional CE-CT, but mitotic count is difficult to be calculated preoperatively. Thus, in our study, we further built and validated a specialized radiomic model to predict mitotic count of GISTs, which showed satisfactory performance in distinguishing high– and low–mitotic count GISTs. After radiomic feature selection, the 14 remaining features included range of intensity values, sphericity (measured the shape in the ROI), voxel value sum, uniformity, local homogeneity (including seven features of inverse difference moment), similarity of the gray levels in neighboring pixels,

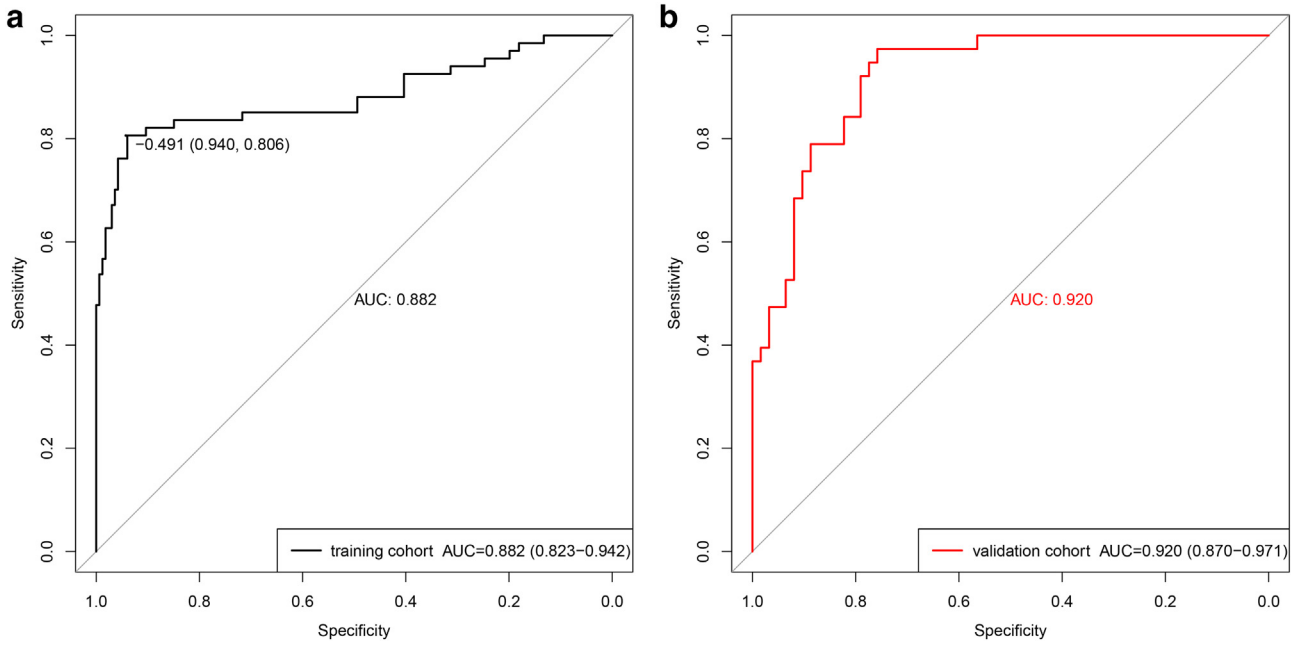

Figure 3. ROC curves of the radiomic model in training set (A) and validation set (B) in the high– and low–malignant potential groups.

and two features of gray level run-length matrix (Table 3). These remaining radiomic features represented an assessment of tumor shape and tumor heterogeneity. Iannicelli et al. [31] investigated the relations between the morphological CE-CT features and mitotic count of GISTs, and they found a statistically significant association between shape of lesion margins and mitotic count: most (90.9%) of lesions with the low mitotic count showed regular margins (P = .016), suggesting that solid lesions with smooth and not crispy borders could be more aggressive than the ones with jagged borders. Moreover, most (81.8%) of lesions with the high mitotic count showed heterogeneous enhancement and necrosis which represented tumor heterogeneity, while there were no statistically significant differences which may be caused by its small sample size (only 44 patients). In addition, it is noteworthy that the radiomic feature, the range of intensity values, remained after radiomic feature selection in both radiomic models for malignancy differentiation (Table 2) and

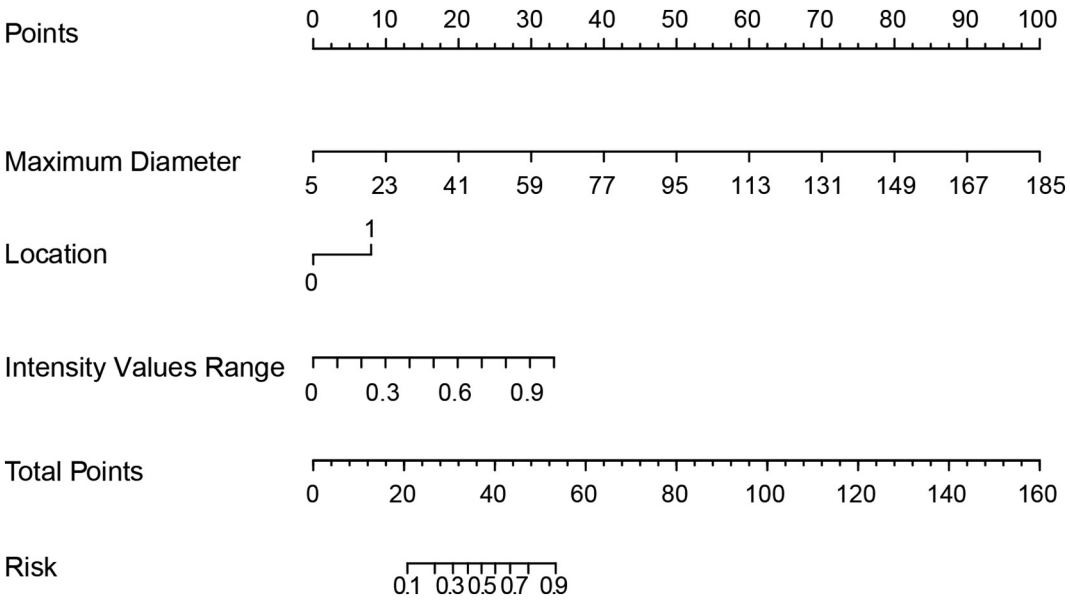

Figure 4. Developed radiomic nomogram. The radiomic model, maximum diameter, range, and tumor location were used for building the radiomic nomogram. The probability of each predictor can be converted into scores according to the first scale "Points" at the top of the nomogram. After adding up the corresponding prediction probability at the bottom of the nomogram is the malignancy of the tumor. The cutoff point of our nomogram is 0.5. The case would be diagnosed as high malignant potential when the total prediction probability is beyond the cutoff point.

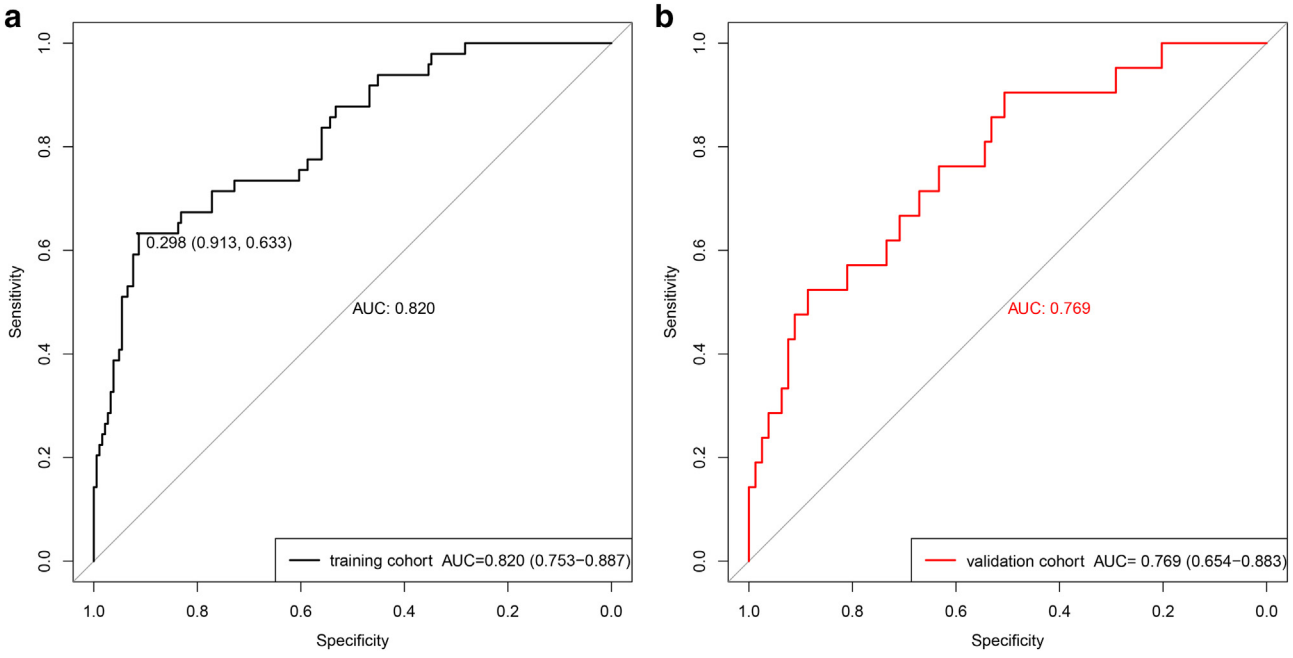

Figure 5. ROC curves of the radiomic model in training set (A) and validation set (B)in the high– and low–mitotic count groups.

mitotic count differentiation (Table 3), which suggested that the radiomic feature, intensity values range, might be a potential imaging biomarker for both mitotic count and malignancy differentiation of GISTs.

In the present study, radiomic features were analyzed using two-dimensional (2D) image in the largest axial plane rather than three-dimensional (3D) images of whole tumor. A previous study demonstrated that single-slice 2D features analysis was sufficient to evaluate the tumor pathology and clinical outcomes due to no significant difference between 2D and 3D texture evaluation of liver metastases [45]. Recently, several studies further demonstrated that 2D radiomics analysis of a single-slice largest cross-sectional image had good performances in preoperatively differentiating malignant grades of colorectal cancer [46] and determining lymph node metastasis in colorectal cancer [18].

However, a limitation of our study is the fact that gene mutations are not considered in this present study. Most GISTs have an activating mutation in tyrosine kinase protein receptor (KIT) gene or platelet-derived growth factor receptor (PDGFRA) gene. Chinese consensus guidelines for the diagnosis and management of GISTs [3] have recommended *c-kit* or *PDGFRA* gene mutational analysis, which is important for diagnosing some difficult cases, predicting the therapeutic effect of targeted drugs and guiding medical decision making. In recent years, radiogenomics, which concentrates on the association between imaging phenotypes and genomics, has emerged and developed in the field of tumor research and received increasing attention [47]. Hence, it is worthwhile to investigate the relationship between radiomic features and different *c-kit* or *PDGFRA* mutation in further radiogenomic study.

In conclusion, our preliminary study showed that the radiomic model had a good performance for preoperatively predicting both malignant potential and mitotic count of GISTs in a noninvasive way. Although promising, these results were preliminary and required validation on a prospective dataset to assess the potential for clinical translation. After validation, the radiomic assessment may become a potential imaging biomarker for GISTs and can be conveniently performed for the preoperative personalized prediction of malignant potential for patients with GISTs.

Funding

This research was supported by Zhejiang Provincial Natural Science Foundation of China under grant no. LQ18H180001, Zhejiang Medicine and Health Science and Technology Program under grant nos. 2017KY080 and 2018KY418, National Key R&D Program of China (2017YFC1308700, 2017YFA0205200, 2017YFC1309100), National Natural Science Foundation of China (81771924, 81227901, 81501616, 81527805, 81671851), the Beijing Natural Science Foundation (L182061), the Bureau of International Cooperation of Chinese Academy of Sciences (173211KYSB20160053), the Instrument Developing Project of the Chinese Academy of Sciences (YZ201502), and the Youth Innovation Promotion Association CAS (2017175).

Appendix A. Supplementary data

Supplementary data to this article can be found online at https://doi.org/10.1016/j.tranon.2019.06.005.

References

[1] Rubin BP, Heinrich MC, and Corless CL (2007). Gastrointestinal stromal tumour. *Lancet* **369**(9574), 1731–1741.

[2] Min KW and Leabu M (2006). Interstitial cells of Cajal (ICC) and gastrointestinal stromal tumor (GIST): facts, speculations, and myths. *J Cell Mol Med* **10**(4), 995–1013.

[3] Li J, Ye Y, Wang J, Zhang B, Qin S, Shi Y, He Y, Liang X, Liu X, and Zhou Y, et al (2017). Chinese consensus guidelines for diagnosis and management of gastrointestinal stromal tumor. *Chin J Cancer Res* **29**(4), 281–293.

[4] Hirota S, Isozaki K, Moriyama Y, Hashimoto K, Nishida T, Ishiguro S, Kawano K, Hanada M, Kurata A, and Takeda M, et al (1998). Gain-of-function

mutations of c-kit in human gastrointestinal stromal tumors. *Science* **279**(5350), 577–580.

[5] Miettinen M, Sobin LH, and Sarlomo-Rikala M (2000). Immunohistochemical spectrum of GISTs at different sites and their differential diagnosis with a reference to CD117 (KIT). *Mod Pathol* **13**(10), 1134–1142.

[6] Baheti AD, Shinagare AB, O'Neill AC, Krajewski KM, Hornick JL, George S, Ramaiya NH, and Tirumani SH (2015). MDCT and clinicopathological features of small bowel gastrointestinal stromal tumours in 102 patients: a single institute experience. *Br J Radiol* **88**(1053)20150085.

[7] Lupescu IG, Grasu M, Boros M, Gheorghe C, Ionescu M, Popescu I, Herlea V, and Georgescu SA (2007). Gastrointestinal stromal tumors: retrospective analysis of the computer-tomographic aspects. *J Gastrointestin Liver Dis* **16**(2), 147–151.

[8] Demetri GD, Benjamin RS, Blanke CD, Blay JY, Casali P, Choi H, Corless CL, Debiec-Rychter M, DeMatteo RP, and Ettinger DS, et al (2007). NCCN Task Force report: management of patients with gastrointestinal stromal tumor (GIST)—update of the NCCN clinical practice guidelines. *J Natl Compr Canc Netw* **5 Suppl 2** S1-29; quiz S30.

[9] Joensuu H (2008). Risk stratification of patients diagnosed with gastrointestinal stromal tumor. *Hum Pathol* **39**(10), 1411–1419.

[10] D'Ambrosio L, Palesandro E, Boccone P, Tolomeo F, Miano S, Galizia D, Manca A, Chiara G, Bertotto I, and Russo F, et al (2017). Impact of a risk-based follow-up in patients affected by gastrointestinal stromal tumour. *Eur J Cancer* **78**, 122–132.

[11] Joensuu H, Eriksson M, Sundby Hall K, Hartmann JT, Pink D, Schutte J, Ramadori G, Hohenberger P, Duyster J, and Al-Batran SE, et al (2012). One vs three years of adjuvant imatinib for operable gastrointestinal stromal tumor: a randomized trial. *JAMA* **307**(12), 1265–1272.

[12] Holdsworth CH, Badawi RD, Manola JB, Kijewski MF, Israel DA, Demetri GD, and Van den Abbeele AD (2007). CT and PET: early prognostic indicators of response to imatinib mesylate in patients with gastrointestinal stromal tumor. *AJR Am J Roentgenol* **189**(6), W324–W330.

[13] Dematteo RP, Gold JS, Saran L, Gonen M, Liau KH, Maki RG, Singer S, Besmer P, Brennan MF, and Antonescu CR (2008). Tumor mitotic rate, size, and location independently predict recurrence after resection of primary gastrointestinal stromal tumor (GIST). *Cancer* **112**(3), 608–615.

[14] Gayed I, Vu T, Iyer R, Johnson M, Macapinlac H, Swanston N, and Podoloff D (2004). The role of 18F-FDG PET in staging and early prediction of response to therapy of recurrent gastrointestinal stromal tumors. *J Nucl Med* **45**(1), 17–21.

[15] Gillies RJ, Kinahan PE, and Hricak H (2016). Radiomics: images are more than pictures, they are data. *Radiology* **278**(2), 563–577.

[16] Yang L, Dong D, Fang M, Zhu Y, Zang Y, Liu Z, Zhang H, Ying J, Zhao X, and Tian J (2018). Can CT-based radiomics signature predict KRAS/NRAS/BRAF mutations in colorectal cancer? *Eur Radiol* **28**(5), 2058–2067.

[17] Huang Y, Liu Z, He L, Chen X, Pan D, Ma Z, Liang C, Tian J, and Liang C (2016). Radiomics signature: a potential biomarker for the prediction of disease-free survival in early-stage (I or II) non–small cell lung cancer. *Radiology* **281**(3), 947–957.

[18] Huang YQ, Liang CH, He L, Tian J, Liang CS, Chen X, Ma ZL, and Liu ZY (2016). Development and validation of a radiomics nomogram for preoperative prediction of lymph node metastasis in colorectal cancer. *J Clin Oncol* **34**(18), 2157–2164.

[19] Dong D, Tang L, Li ZY, Fang MJ, Gao JB, Shan XH, Ying XJ, Sun YS, Fu J, and Wang XX, et al (2019). Development and validation of an individualized nomogram to identify occult peritoneal metastasis in patients with advanced gastric cancer. *Ann Oncol* **30**(3), 431–438.

[20] Zhang B, Tian J, Dong D, Gu D, Dong Y, Zhang L, Lian Z, Liu J, Luo X, and Pei S, et al (2017). Radiomics features of multiparametric MRI as novel prognostic factors in advanced nasopharyngeal carcinoma. *Clin Cancer Res* **23**(15), 4259–4269.

[21] Wang S, Shi J, Ye Z, Dong D, Yu D, Zhou M, Liu Y, Gevaert O, Wang K, and Zhu Y, et al (2019). Predicting EGFR mutation status in lung adenocarcinoma on computed tomography image using deep learning. *Eur Respir J* **53**(3).

[22] Sandrasegaran K, Rajesh A, Rushing DA, Rydberg J, Akisik FM, and Henley JD (2005). Gastrointestinal stromal tumors: CT and MRI findings. *Eur Radiol* **15**(7), 1407–1414.

[23] Choi H (2008). Response evaluation of gastrointestinal stromal tumors. *Oncologist* **13**(Suppl 2), 4–7.

[24] Haralick R, Shanmugam K, Dinstein I, Haralick RM, and Shanmuga K (1973). Dinstein I. Textural features for image classification. *IEEE Trans Syst Man Cybern* **3**, 610–621.

[25] Galloway M (1974). Texture analysis using gray level run lengths; 1974 .

[26] Tang X (1998). Texture information in run-length matrices. *IEEE Trans Image Process* **7**(11), 1602–1609.

[27] Gstoettner M, Sekyra K, Walochnik N, Winter P, Wachter R, and Bach CM (2007). Inter- and intraobserver reliability assessment of the Cobb angle: manual versus digital measurement tools. *Eur Spine J* **16**(10), 1587–1592.

[28] Ding C and Peng H (2005). Minimum redundancy feature selection from microarray gene expression data. *J Bioinform Comput Biol* **3**(2), 185–205.

[29] DeMatteo RP, Lewis JJ, Leung D, Mudan SS, Woodruff JM, and Brennan MF (2000). Two hundred gastrointestinal stromal tumors: recurrence patterns and prognostic factors for survival. *Ann Surg* **231**(1), 51–58.

[30] George S, Reichardt P, Lechner T, Li S, Cohen DP, and Demetri GD (2012). Hypertension as a potential biomarker of efficacy in patients with gastrointestinal stromal tumor treated with sunitinib. *Ann Oncol* **23**(12), 3180–3187.

[31] Iannicelli E, Carbonetti F, Federici GF, Martini I, Caterino S, Pilozzi E, Panzuto F, Briani C, and David V (2017). Evaluation of the relationships between computed tomography features, pathological findings, and prognostic risk assessment in gastrointestinal stromal tumors. *J Comput Assist Tomogr* **41**(2), 271–278.

[32] Otomi Y, Otsuka H, Morita N, Terazawa K, Furutani K, Harada M, and Nishitani H (2010). Relationship between FDG uptake and the pathological risk category in gastrointestinal stromal tumors. *J Med Invest* **57**(3–4), 270–274.

[33] Yoshikawa K, Shimada M, Kurita N, Sato H, Iwata T, Morimoto S, Miyatani T, Kashihara H, Takasu C, and Matsumoto N (2013). Efficacy of PET-CT for predicting the malignant potential of gastrointestinal stromal tumors. *Surg Today* **43**(10), 1162–1167.

[34] Tokumoto N, Tanabe K, Misumi T, Fujikuni N, Suzuki T, and Ohdan H (2014). The usefulness of preoperative 18FDG positron-emission tomography and computed tomography for predicting the malignant potential of gastrointestinal stromal tumors. *Dig Surg* **31**(2), 79–86.

[35] Wong CS, Gong N, Chu YC, Anthony MP, Chan Q, Lee HF, Chu KM, and Khong PL (2012). Correlation of measurements from diffusion weighted MR imaging and FDG PET/CT in GIST patients: ADC versus SUV. *Eur J Radiol* **81**(9), 2122–2126.

[36] Fletcher CD, Berman JJ, Corless C, Gorstein F, Lasota J, Longley BJ, Miettinen M, O'Leary TJ, Remotti H, and Rubin BP, et al (2002). Diagnosis of gastrointestinal stromal tumors: a consensus approach. *Hum Pathol* **33**(5), 459–465.

[37] Miettinen M and Lasota J (2006). Gastrointestinal stromal tumors: pathology and prognosis at different sites. *Semin Diagn Pathol* **23**(2), 70–83.

[38] von Mehren M, Randall RL, Benjamin RS, Boles S, Bui MM, Ganjoo KN, George S, Gonzalez RJ, Heslin MJ, and Kane III JM, et al (2018). Soft tissue sarcoma, version 2.2018, NCCN clinical practice guidelines in oncology. *J Natl Compr Canc Netw* **16**(5), 536–563.

[39] Joensuu H, Vehtari A, Riihimaki J, Nishida T, Steigen SE, Brabec P, Plank L, Nilsson B, Cirilli C, and Braconi C, et al (2012). Risk of recurrence of gastrointestinal stromal tumour after surgery: an analysis of pooled population-based cohorts. *Lancet Oncol* **13**(3), 265–274.

[40] von Mehren M, Randall RL, Benjamin RS, Boles S, Bui MM, Conrad 3rd EU, Ganjoo KN, George S, Gonzalez RJ, and Heslin MJ, et al (2016). Soft tissue sarcoma, version 2.2016, NCCN clinical practice guidelines in oncology. *J Natl Compr Canc Netw* **14**(6), 758–786.

[41] Nishida T, Goto O, Raut CP, and Yahagi N (2016). Diagnostic and treatment strategy for small gastrointestinal stromal tumors. *Cancer* **122**(20), 3110–3118.

[42] Tanaka J, Oshima T, Hori K, Tomita T, Kim Y, Watari J, Oh K, Hirota S, Matsumoto T, and Miwa H (2010). Small gastrointestinal stromal tumor of the stomach showing rapid growth and early metastasis to the liver. *Dig Endosc* **22**(4), 354–356.

[43] Miettinen M, Makhlouf H, Sobin LH, and Lasota J (2006). Gastrointestinal stromal tumors of the jejunum and ileum: a clinicopathologic, immunohistochemical, and molecular genetic study of 906 cases before imatinib with long-term follow-up. *Am J Surg Pathol* **30**(4), 477–489.

[44] Nishida T, Blay JY, Hirota S, Kitagawa Y, and Kang YK (2016). The standard diagnosis, treatment, and follow-up of gastrointestinal stromal tumors based on guidelines. *Gastric Cancer* **19**(1), 3–14.

[45] Lubner MG, Stabo N, Lubner SJ, del Rio AM, Song C, Halberg RB, and Pickhardt PJ (2015). CT textural analysis of hepatic metastatic colorectal cancer: pre-treatment tumor heterogeneity correlates with pathology and clinical outcomes. *Abdom Imaging* **40**(7), 2331–2337.

[46] Huang X, Cheng Z, Huang Y, Liang C, He L, Ma Z, Chen X, Wu X, Li Y, and Liang C, et al (2018). CT-based radiomics signature to discriminate high-grade from low-grade colorectal adenocarcinoma. *Acad Radiol* **25**(10), 1285–1297.

[47] Mazurowski MA (2015). Radiogenomics: what it is and why it is important. *J Am Coll Radiol* **12**(8), 862–866.